SLAC-PUB-3130
May 1983
(M)

THE USE OF NITROGEN LASER FOR OBSERVATION OF SPACE CHARGE EFFECTS IN DRIFT CHAMBERS AND DEVELOPMENT OF HIGH PRECISION VERTEX CHAMBERS*

J. VA'VRA
Stanford Linear Accelerator Center
Stanford University, Stanford, California 94305

ABSTRACT

A two-stage nitrogen laser has been built and is presently being used to investigate properties of drift chambers. In this paper we present the measured parameters of this laser, the results of a study of the double track separation in a drift chamber of jet design and a measurement of the saturation effects in this chamber as a function of total gain. An understanding of the saturation effects is important for drift chambers with multiple hit capability. The laser technique reported here represents a major improvement in the simplicity of investigation of the double track separation and saturation effects. In addition, we have demonstrated a usefulness of this kind of laser in a development of high precision drift chambers working in a resolution range of $\sim 20-30\ \mu m$.

Long Version Submitted to Nuclear Instruments and Methods

and

Short Version Presented at the Nuclear Science Symposium,
Washington, D.C., October 20-22, 1982.

---

* Work supported by the Department of Energy, contract DE-AC03-76SF00515.

1. INTRODUCTION

It is believed that in the future, experiments will be run with very high track densities. To date, there have been great efforts to improve the double hit capability of drift chambers by digitizing the waveform every 5-10 ns [1]. Such systems are clearly very expensive and care has to be exercised in the prototyping stage to ensure a full understanding of the system. We believe that lasers, such as one presented in this paper can play an important role in the early stages of development [2-9]. For instance, we have used it to check a Monte Carlo program to predict expected waveforms [12]. It can be used to study and tune the electronics at a very early stage. In this paper, we present a simple method to measure saturation effects, in which the cloud of positive ions produced by an avalanche can seriously affect the measurement of charge from a second track near the first track or even late arriving charge from the same track. Similar measurement in a particle beam is next to impossible.

2. DESCRIPTION OF THE LASER AND ITS PERFORMANCE

A pulsed, two-stage nitrogen laser has been built at SLAC. The original design* has been modified to improve the spark gap trigger as well as the rf noise performance. The main advantages of this particular design are small spot size and small divergence of the laser beam, very short burst duration and, as a result, a large power density per unit of time and of area. It belongs to a category of nitrogen lasers suitable for precise bench experiments rather than for a continuous long term monitoring of large experiments.

The laser obtains good divergence from the fact that it is optically long. This is achieved by combining two lasers together. The beam coming from the first cavity

*MOPA 1000 from Multilasers, Grand-Sacounex, Switzerland.

is returned through the right angle prism (BK-7 glass)* into the second cavity - see fig. 1. The timing of the two cavities is done empirically through an adjustment of the cavity gaps. The second cavity is made to lase by a leading edge of the incoming wave of photons. The solid angle acceptance of the second cavity eliminates large unwanted light reflections from the lasing electrodes in the first cavity, which are present in miniature versions of this type of laser (MOPA-400). The present work does not employ an optical expander between the two cavities to further improve the beam divergence [2].

We used a RETICON linear CCD array (RL256C) to measure the beam profiles under various conditions - see figs. 2 through 5. The beam was attenuated using neutral density filters.† The beam divergence was obtained by measuring spots at different distances from the laser. The smallest achieved spot size was $\sim$ 50 μm vertically and $\sim$ 75 μm horizontally (FWHM) using an f = 10 cm lens† with a pinhole in front of it. For measurements reported in this paper we used f = 100 cm and f = 50 cm lenses.† The energy of the laser was measured using an EG&G UV-444B diode. For the trigger in the precision timing measurements, we used an EG&G FND-100 diode and for the burst duration measurement, we used an ITT F-4000 (S-5) biplanar vacuum photodiode. Typical measured performance is listed in table I.

3. DETECTOR TO MEASURE SATURATION EFFECTS

The tracks were generated in a jet chamber prototype [10] operating at normal pressure and with 90% Argon + 9% CO_2 + 1% CH_4 gas. The chamber had 47

---

* Made by CVI laser Corporation, Albuquerque, New Mexico 87112.

† Standard fused silica quartz made by Melles Griot or Rolyn Optics Companies.

sense wires, each sampling 1.5 cm of track length. Between the 20 μm diameter sense wires are 125 μm diameter guard wires. The chamber operated with the cathode at ground potential and the sense and guard wires at positive voltage. Different gains were obtained by varying the voltage on the guard wires and the voltage on the sense wires. The wires were arranged so that the vertical edge of the beam was alligned with a drift direction. The chamber was connected to an amplifier with a $\sim$ 10 ns rise-time and $\sim$ 50 ns fall-time response to an impulse charge.

4. EXPERIMENTAL RESULTS

The experimental setup can be seen in fig. 1. Figures 6 through 8 show typical pulse height distributions in the chamber, the diode and their correlations. To create double tracks in the chamber, we reflected the beam through an orthogonal system of two mirrors.* The mirror system was mounted on a precision table allowing transverse and rotational motion. Figure 9 shows a typical single track as measured on several wires in the chamber. The pictures are multiple exposures of typically 40 shots. The chamber operated at a total gain of $\sim 2 \times 10^5$ and the ionization created by the laser was about three times that of a minimum ionizing particle. We cannot use the observation of relative pulse height uniformity along the laser track as a indication of uniform ionization yield, because the chamber operated at rather large gain during this measurement. Figure 10 shows the typical double tracks. The total length is about 1.5 m. Figures 11 and 12 show double tracks on wire #4 as a function of a distance between the two tracks, with and without a two zero-pole filters [11] to suppress the 1/t tail from positive ion motion. The two zero-pole filters were tuned for maximum tail cancellation while the laser was running. Although the results were

* Square flat mirror (Pyrex) made by Melles Griot Company.

better with two filters, one would obtain a reasonable tail cancellation with only one zero-pole filter. It can be seen that it is possible to separate two tracks down to 2-3 mm if the waveform is digitized every $\sim$ 10 ns. This would be improved in a chamber with smaller wire spacing. In the case of real particles, clustering effects will tend to confuse some fraction of hits.

Figure 13 represents the concept of the measurement of saturation effects. The tracks are separated by 10 mm and we used the zero-pole filters to clearly determine the amplitude of the second pulse. By rotating the system of two mirrors, we find a position where the second pulse is at a minimum in amplitude. At that point, we fix the rotating table and proceed to vary the gain in the chamber. At lower gains, one retains the full amplitude of the second pulse. Figure 14 shows the results of the saturation measurement. Two different sets of points were obtained by either lowering the gain through the sense wire or guard wire voltages. Either of these two conditions will alter the collecting characteristics of the chamber. Nevertheless, in both cases one gets the same result. To minimize the spot size, the two mirrors were located at the focus plane of an f = 100 cm quartz lens and wire #4 was 24.5 cm from the focus. The results were insensitive to lens position. As can be seen in fig. 3, the vertical distribution does not change near the focus of the f = 100 cm lens. Similar results were obtained when the wire plane was between the two tracks, i.e., the two avalanches came from opposite directions toward the wire. However, the onset of the saturation came at a voltage $\sim$ 100 volts higher.

5. RESULTS WITH HIGH PRESSURE CHAMBER

We are presently using the laser to investigate properties of a high pressure drift chamber. With the f = 50 cm lens and a small prototype of a micro-jet chamber [12], we succeeded in measuring tracks as close as 1 mm from the sense wires. Figure 15

shows the geometry of the micro-jet chamber and fig. 16 shows the FND-100 diode start pulse and the laser generated drift chamber pulse. The chamber operated at 7.2 atm with 90% Ar + 9% CO_2 + 1% CH_4 gas, and we used an amplifier with a 2-3 ns rise-time response to an impulse charge [11,12]. The number of photons in the laser beam in fig. 16 corresponds to about 10^{14}/burst. The measured threshold to create the laser ionization corresponds to about 5×10^{12} photons/burst.

Figure 17 shows the calibration of the chamber using the laser and the Fe^{55} source. The ratio of the laser ionization yield and the Fe^{55} source signal was found to be independent of pressure. Figure 18 shows the relative laser ionization yield compared to the minimum ionizing particle, obtained from the Fe^{55} source calibration. This result is consistent with an explanation that the impurities causing the laser ionization are not coming from the gas bottle, but they are present already initially. The chamber was operated at lower gain during this measurement to ensure linearity.

Figure 19 shows the resolution results achieved with the laser beam. The best achieved laser results indicate a three wire resolution $\sim 24\ \mu m$ for an ionization yield ~ 3 times that of a minimum ionizing particle. This corresponds to a timing resolution of about 0.82 ns in 90% Argon + 10% C_4H_{10} gas. The contribution of electronics alone to the three wire resolution was measured to be ~ 61 psec, which is equivalent to $\sim 2.1\ \mu$m – see fig. 19(e). The laser result was slightly worse compared to the resolution obtained in the particle beam [12], presumably due to a presence of slightly larger noise from the spark gap – see fig. 16. The spark gap noise necessitated to increase the threshold from 30 mV to 100 mV. The stability of an edge of the laser has been measured by fitting a straight line to three wires and the error in intercept is consistent with $\sim 25\ \mu m$ resolution – see fig. 19(a). Comparison of figs. 19(b) and 19(c) indicates that the resolution improves if we lower E/p. This points to a need to bias the guard wires to a negative voltage. The 90% Argon + 90% CO_2 + 1% CH_4

gas gave us a worse resolution – see fig. 19(d). We interpret this as a result of larger diffusion at this value of E/p. This is our preferred gas, because of its lower tendency to polymerize. However, it requires to operate at lower E/p. We see this dependence in our data. Figures 19(b)-19(d) correspond to a comparable total gain in the chamber $(1 - 2 \times 10^5)$ and the same laser beam intensity. These results indicate a usefulness of this type of laser in a development of high precision drift chambers. It will allow to tune some of the most intrinsic parameters.

6. FINAL COMMENTS

Our experience with this type of laser indicates that it can be made reliable. However, because of using a spark gap, periodic downtimes are to be expected. For this reason, we believe, this is not the type of laser to use for long-term monitoring of large experiments.

The rf shield should be properly designed right from the beginning, employing proper rf gaskets, feed-throughs, etc. In our case, we built a high voltage pulser right in the laser box, and used three Faraday cages around the laser. Even then some additional shielding was needed at the detector end.

ACKNOWLEDGEMENTS

We would like to thank Dr. L. Keller and H. Weidner for interest and support during this project. We appreciate discussions with Drs. H. Hilke and C. K. Sinclair. We thank Dr. D. Freytag for help with his CCD array. We would like to thank K. Hughes for excellent machining work and J. Nicol for help during the construction of the laser.

REFERENCES

[1] W. Farr, R. D. Heuer and A. Wagner, IEEE Trans. on Nucl. Sci. NS-30 (1983).

[2] J. C. Guo, F. G. Hartjest and J. Konijn, NIKHEF H/82-5.

[3] H. Anderhub, M. J. Devereux and P. G. Seiler, Nucl. Instrum. Methods 166 (1979) 581 and 176 (1980) 323.

[4] J. Bourotte and B. Sadoulet, Nucl. Instrum. Methods 173 (1980) 463.

[5] H. Hilke, Nucl. Instrum. Methods 174 (1980) 145.

[6] M. DeSalvo and R. DeSalvo, Nucl. Instrum. Methods 201 (1982) 357.

[7] H. M. Fischer, A. Hegerath, E. Hilger and A. Jocksch, 1983 Wirechamber Conference, Vienna, Austria.

[8] J. Konijn and F. Hartjes, 1983 Wirechamber Conference, Vienna, Austria.

[9] C. Raine, K. W. D. Ledingham and K. M. Smith, 1983 Wirechamber Conference, Vienna, Austria.

[10] J. Va'vra and D. Rust, SLAC-PUB-2635 (1980).

[11] R. A. Boie, A. T. Hrisoho and P. Rehak, Nucl. Instrum. Methods 192 (1982) 365-374.

[12] J. Va'vra, Contribution to 1983 Wirechamber Conference, Vienna, Austria, and SLAC-PUB-3045 (1983).

TABLE I

Beam Divergence	$\sim$ 0.7 mrad vertical
	$\sim$ 1.1 mrad horizontal
Beam Size (FWHM)	
(a) Unfocused beam at exit	$\sim$ 0.6 mm vertical
	$\sim$ 2.1 mm horizontal
(b) At focus of f = 50 cm lens	$\sim$ 250 μm vertical
(c) At focus of f = 100 cm lens	$\sim$ 375 μm vertical
Smallest Achieved Beam Size (FWHM)	
(At focus of f = 10 cm lens and	$\sim$ 50μm vertical
Pinhole restriction)	$\sim$ 75μm horizontal
Positional Edge Stability	
(At focus of f = 50 cm lens)	$<$ 25 μm vertical
Light Yield Stability (σ)	$\leq$ 10%
Pulse Time Duration	$\leq$ 0.5 ns
Typical Light Output Energy/Burst	$\sim 50 - 100\ \mu J$
Total Stored Electrical Energy/Burst	$\sim$ 0.34 J
Laser Wavelength	337 nm
Typical Operating Pulse Frequency	1-5 Hz
Typical Operating High Voltage	$\sim \pm$17 kV DC

FIGURE CAPTIONS

1. Experimental setup to observe the double tracks.
2. (a) Unfocused vertical beam shape 53 cm away from the exit of the laser box. (Point to point distance is 25.4 μm.) (b) Unfocused horizontal beam shape 24 cm away from the exit of the laser box.
3. Beam shape obtained using f = 100 cm lens; (a) vertical at focus, (b) vertical at focus -9 cm, (c) vertical at focus +20 cm, and (d) horizontal at focus.
4. Vertical beam shape at focus of f = 50 cm lens; (a) single shot, and (b) 40 shots to see reproducibility.
5. Smallest achieved beam size at a focus of f = 10 cm lens; (a) vertical, and (b) horizontal. (Point to point distance is 25.4 μm.)
6. Pulse height distribution in the chamber.
7. Pulse height distribution in the monitoring diode.
8. Correlation of pulse height between the chamber and diode.
9. (a)-(e) Single track in the chamber, 200 mV/div, 100 ns/div, 40 exposures, no zero-pole filter, wires 4, 12, 24, 36, 44.
10. (a)-(e) Double tracks 9 mm apart, 200 mV/div, 100 ns/div, no zero-pole filter, wires 4, 16, 24, 36, 44. Total length of ionization corresponds to $\sim$ 1.5 m long track.
11. (a)-(e) Double tracks on wire #4 as a function of their distance, 200 mV/div, 100 ns/div, no zero-pole filters, distances 2, 3, 4, 5, 10 mm.
12. (a)-(e) The same as in fig. 11, except 50 mV/div and amplifier with two zero-pole filters.
13. Principle of the saturation effects measurement.
14. The relative saturation effect as a function of total gain.

15. The micro-jet chamber prototype.

16. The laser induced drift pulse and the diode pulse at 7.2 atm, $V_{side} = -6$ kV, $V_{guard} = -1$ kV and 90% Ar + 90% CO_2 + 1% CH_4.

17. The calibration of the micro-jet chamber using the laser and the Fe^{55} source.

18. Relative ionization yield of the laser and the minimum ionizing particle as a function of the gas pressure in the micro-jet chamber.

19. (a) Resolution in an intercept of the straight line fit ($y = a+bx$). (b) Three-wire resolution obtained in the micro-jet chamber using the laser beam (90% Argon+ 10% C_4H_{10}, 7.2 atm, $V_{side} = -4.55$ kV, $V_{guard} = -1.0$ kV). (c) In 90% Argon + 10% C_4H_{10}, 7.2 atm, V_{side} = -7.0 kV, $V_{guard} = 0$ kV. (d) In 90% Argon + 90% CO_2 + 1% CH_4, 7.2 atm, V_{side} = -6.0 kV, V_{guard} = -1.0 kV. (e) Electronic resolution obtained by pulsing 3 amplifiers.

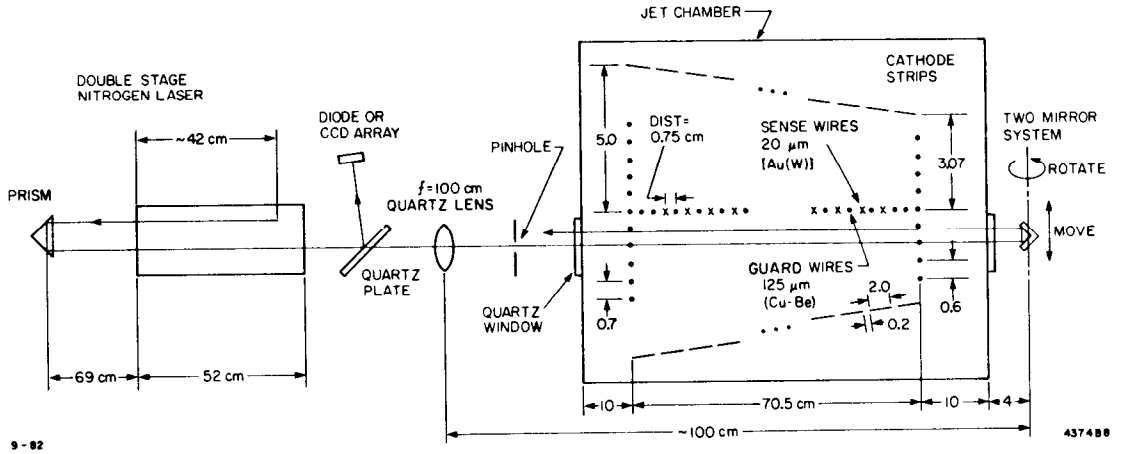
JET CHAMBER
CATHODE STRIPS
DOUBLE STAGE NITROGEN LASER
~42 cm
DIODE OR CCD ARRAY
PINHOLE
PRISM
f=100 cm QUARTZ LENS
5.0
DIST= 0.75 cm
SENSE WIRES 20 μm [Au(W)]
3.07
TWO MIRROR SYSTEM
ROTATE
MOVE
QUARTZ PLATE
QUARTZ WINDOW
GUARD WIRES 125 μm (Cu-Be)
2.0
0.2
0.6
0.7
69 cm
52 cm
10
70.5 cm
10
4
~100 cm
9-82
437488

Fig. 1

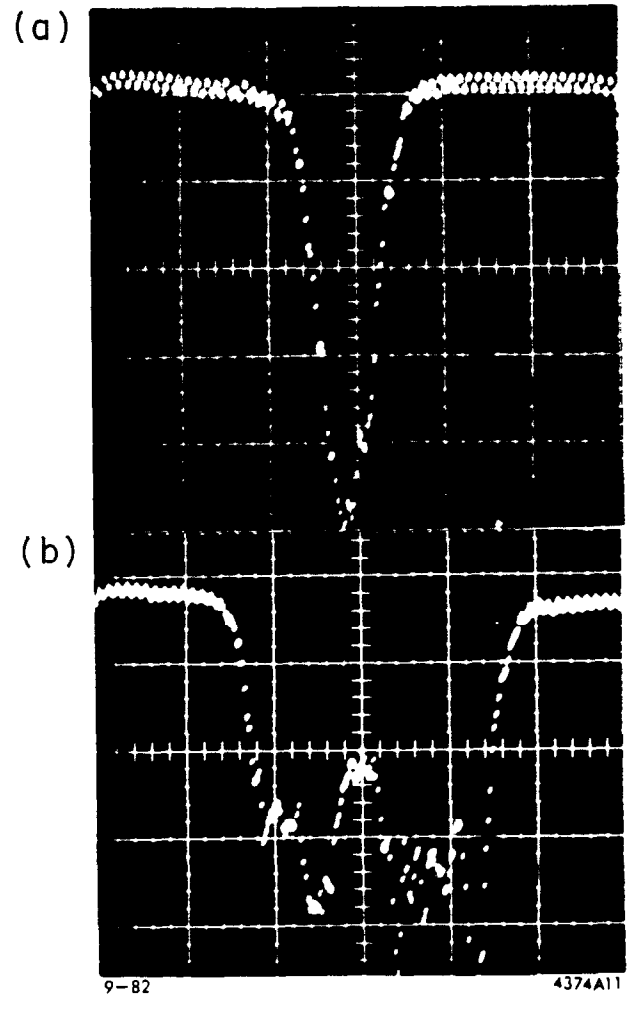

Fig. 2

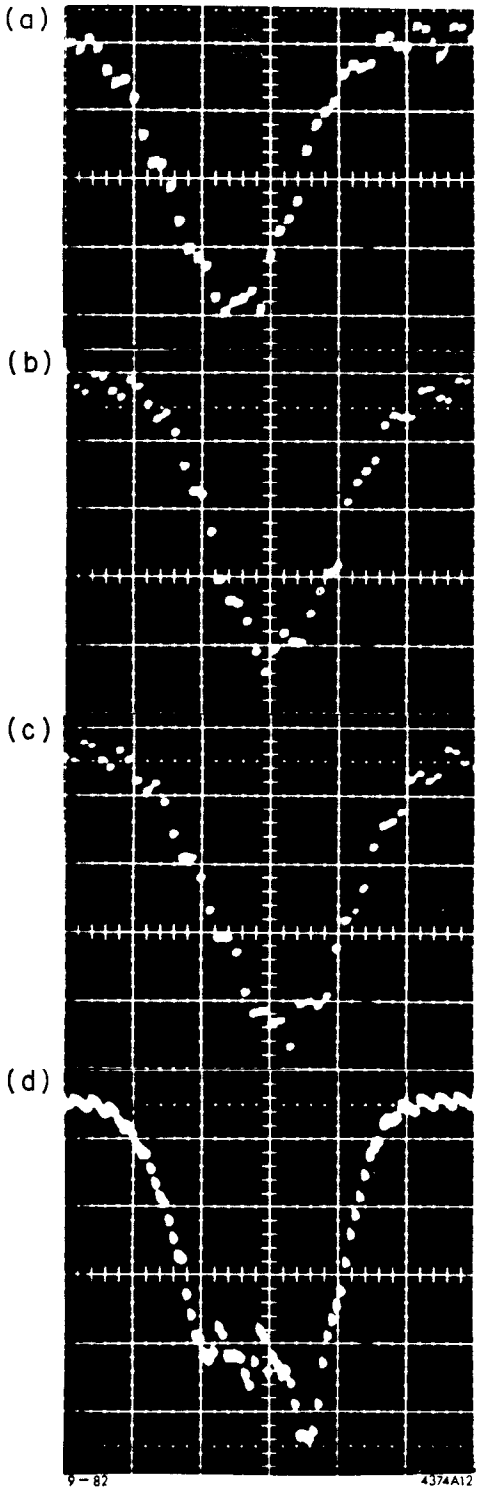

Fig. 3

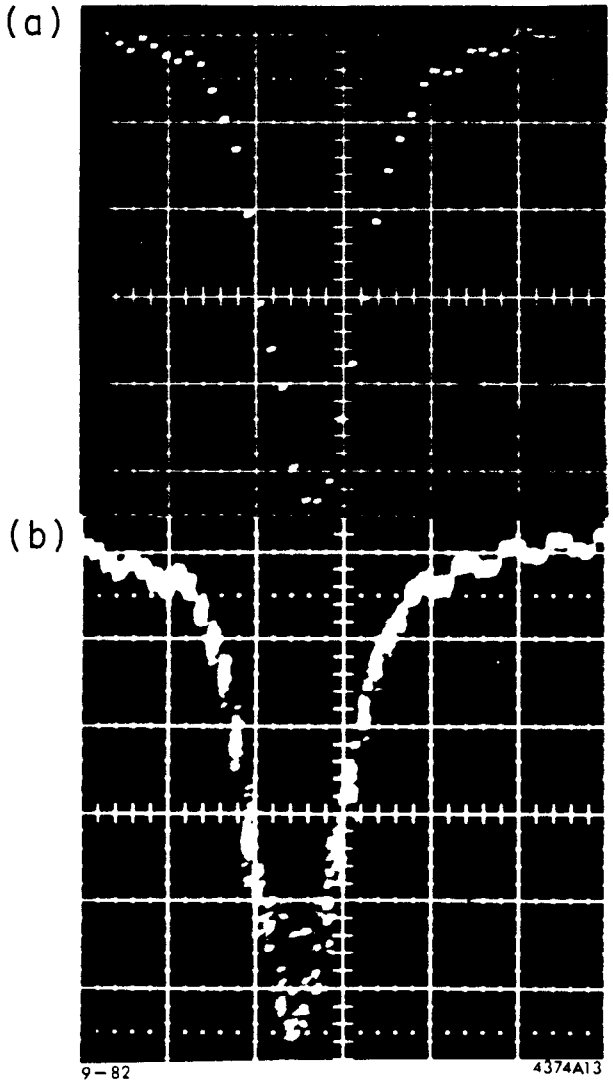

Fig. 4

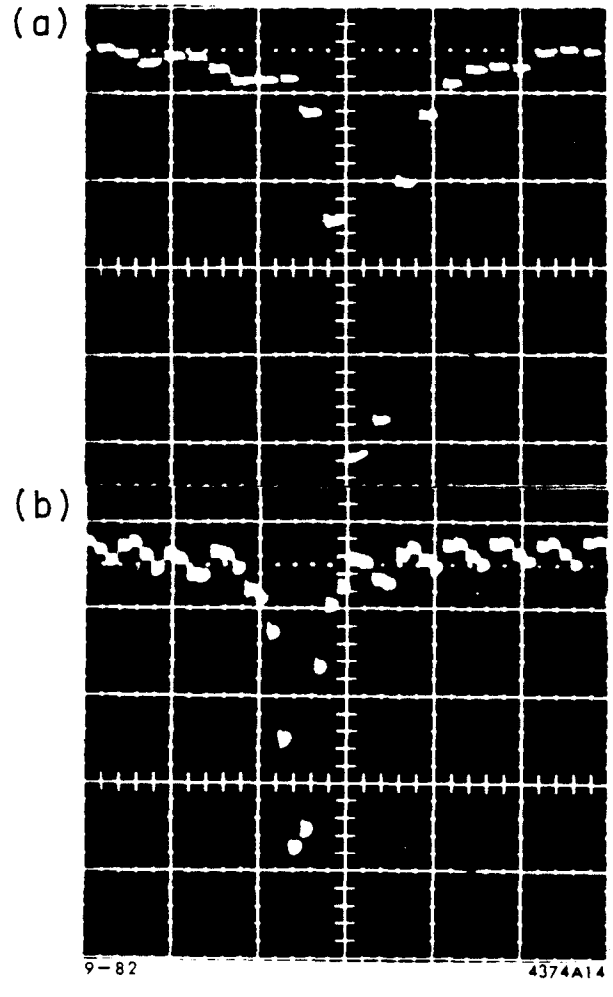

Fig. 5

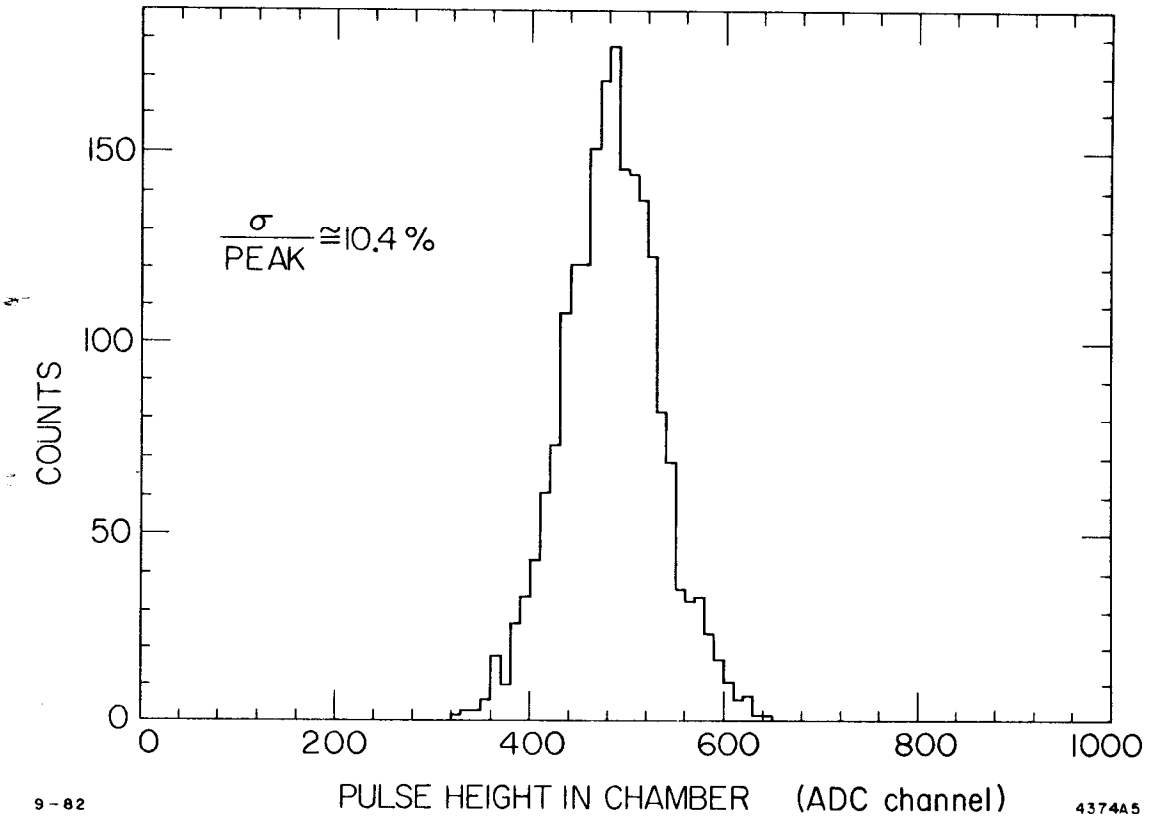
150
100
50
0
COUNTS
σ/PEAK ≅10.4 %
0
200
400
600
800
1000
PULSE HEIGHT IN CHAMBER (ADC channel)
9-82
4374A5

Fig. 6

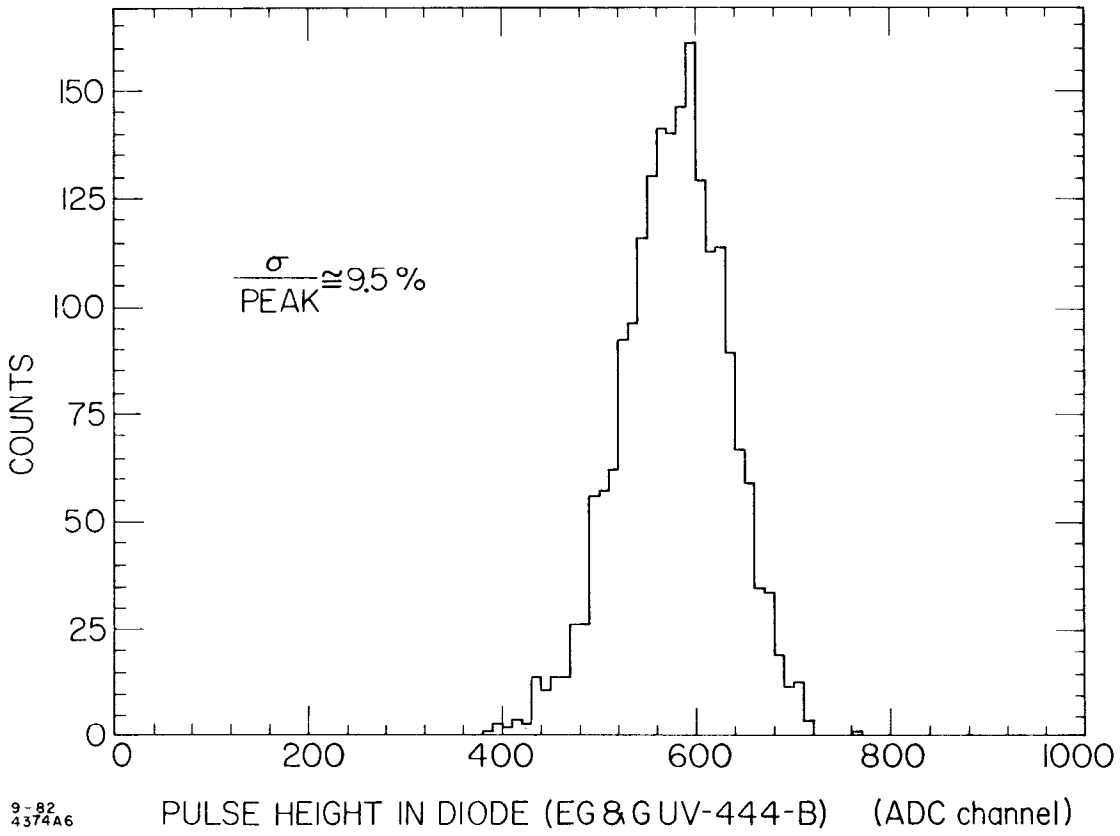
150
125
100
75
50
25
0
COUNTS
σ/PEAK ≅ 9.5 %
0
200
400
600
800
1000
9-82
4374A6
PULSE HEIGHT IN DIODE (EG&G UV-444-B) (ADC channel)

Fig. 7

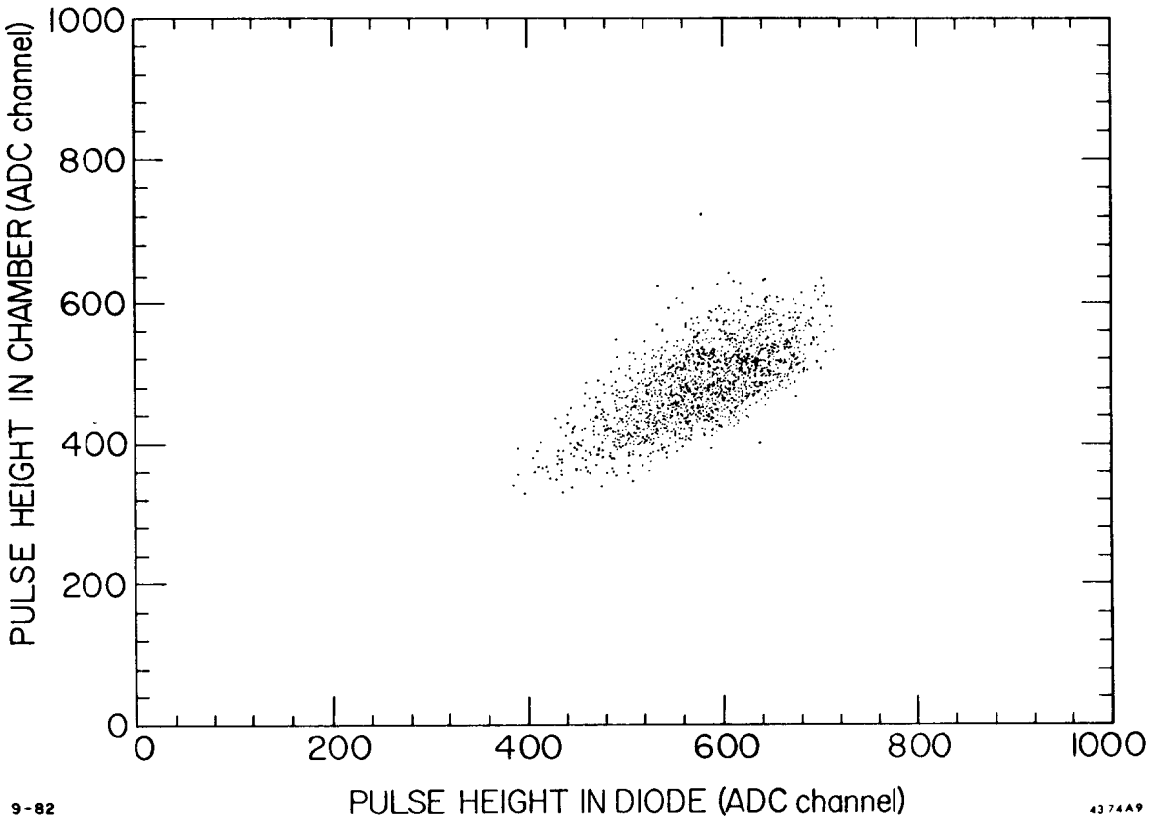
PULSE HEIGHT IN CHAMBER (ADC channel)
1000
800
600
400
200
0
0
200
400
600
800
1000
PULSE HEIGHT IN DIODE (ADC channel)
9-82
4374A9

Fig. 8

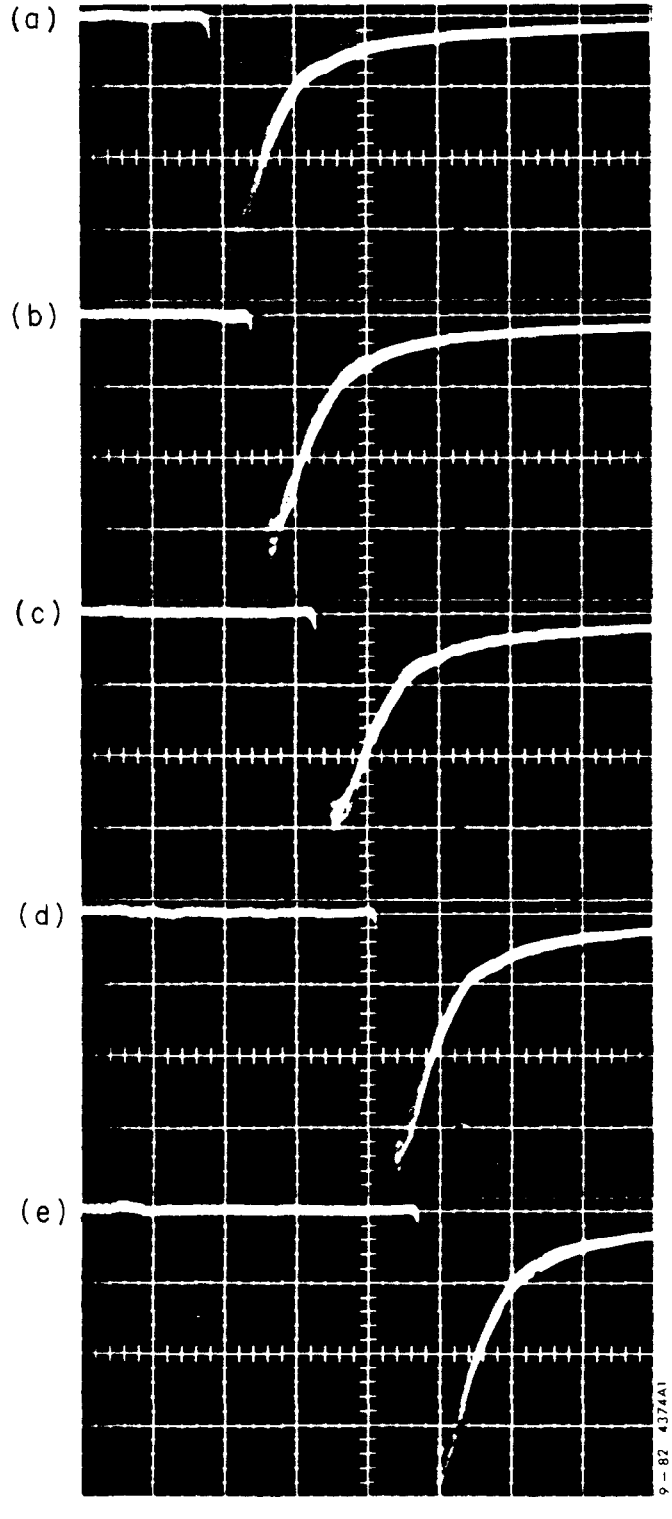

Fig. 9

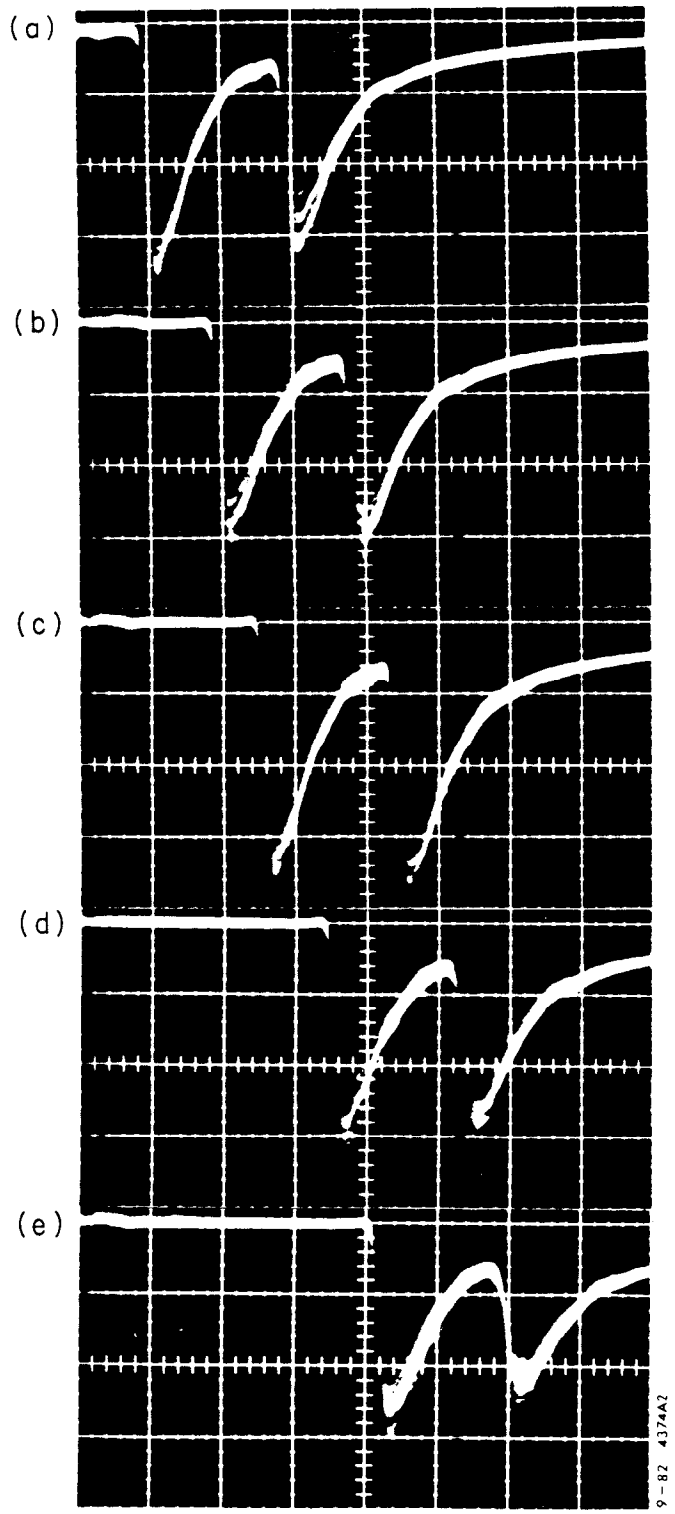

Fig. 10

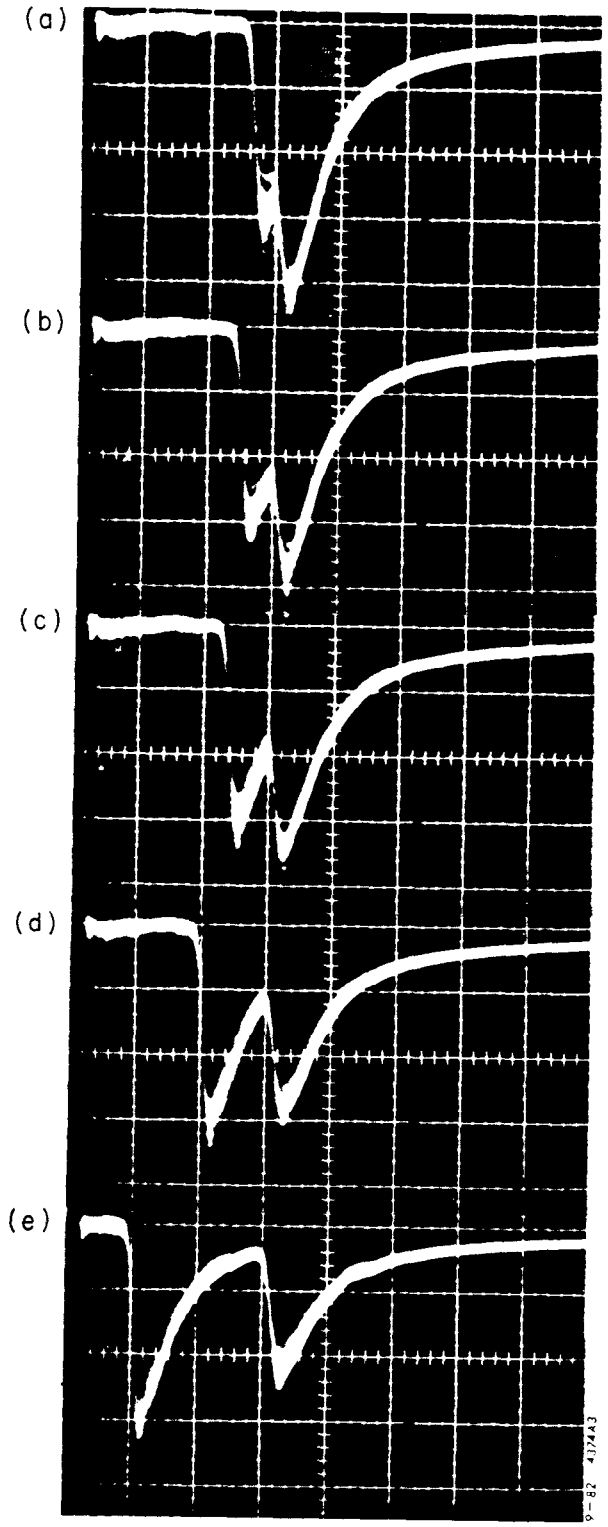

Fig. 11

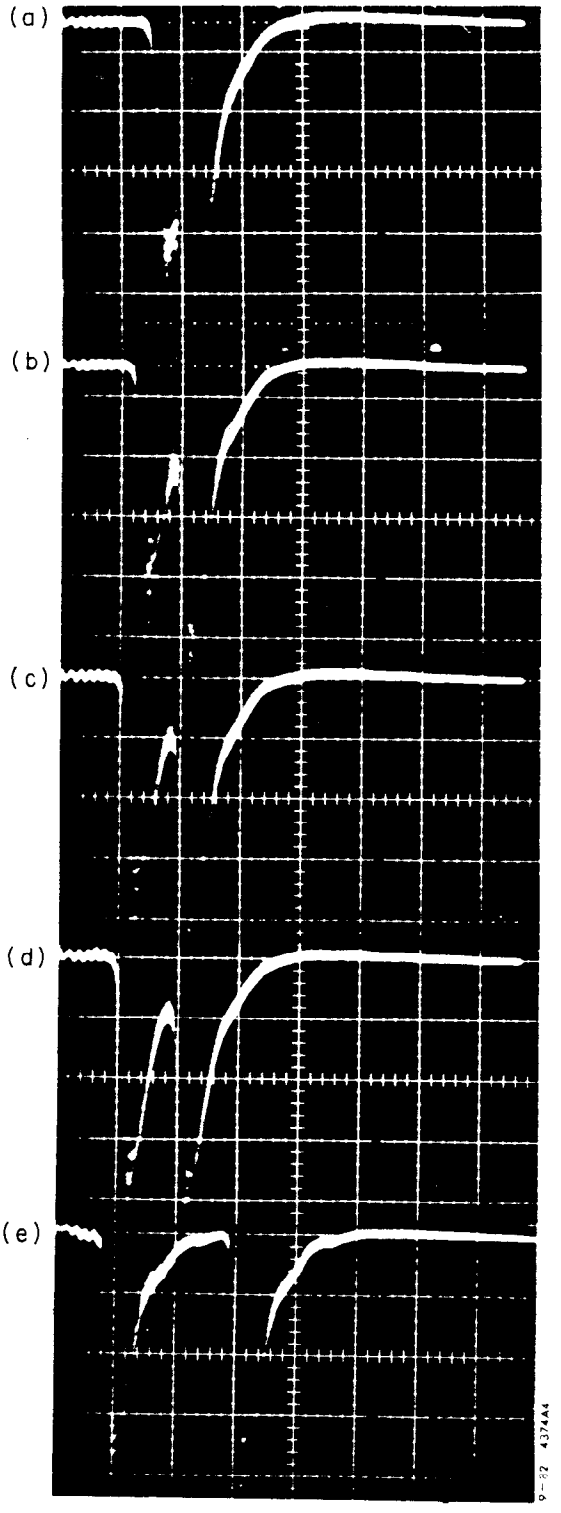

Fig. 12

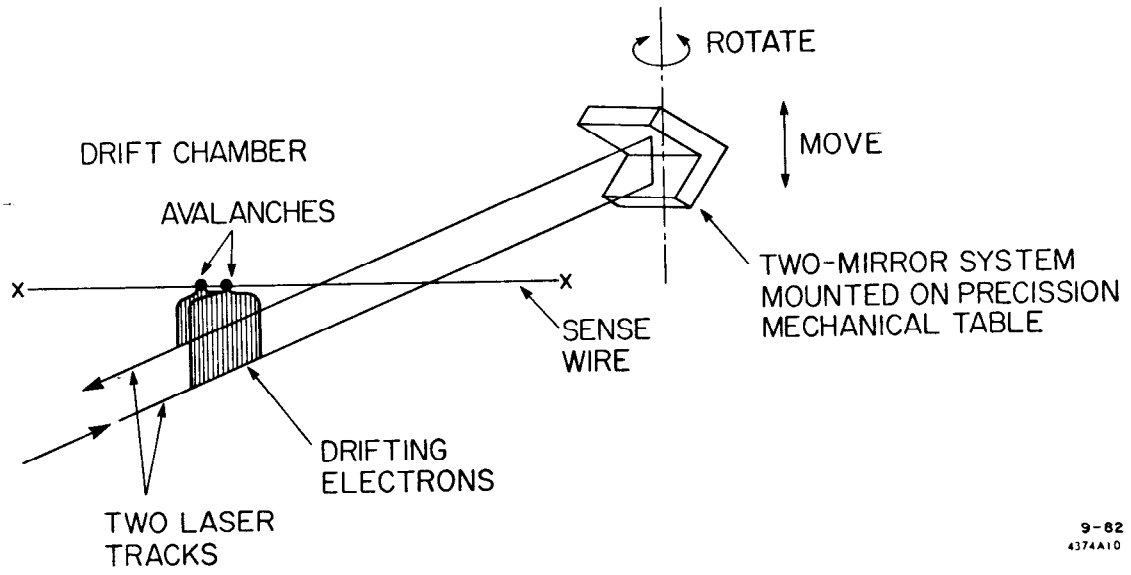
ROTATE
MOVE
DRIFT CHAMBER
AVALANCHES
X
X
SENSE
WIRE
TWO-MIRROR SYSTEM
MOUNTED ON PRECISSION
MECHANICAL TABLE
DRIFTING
ELECTRONS
TWO LASER
TRACKS
9-82
4374A10

Fig. 13

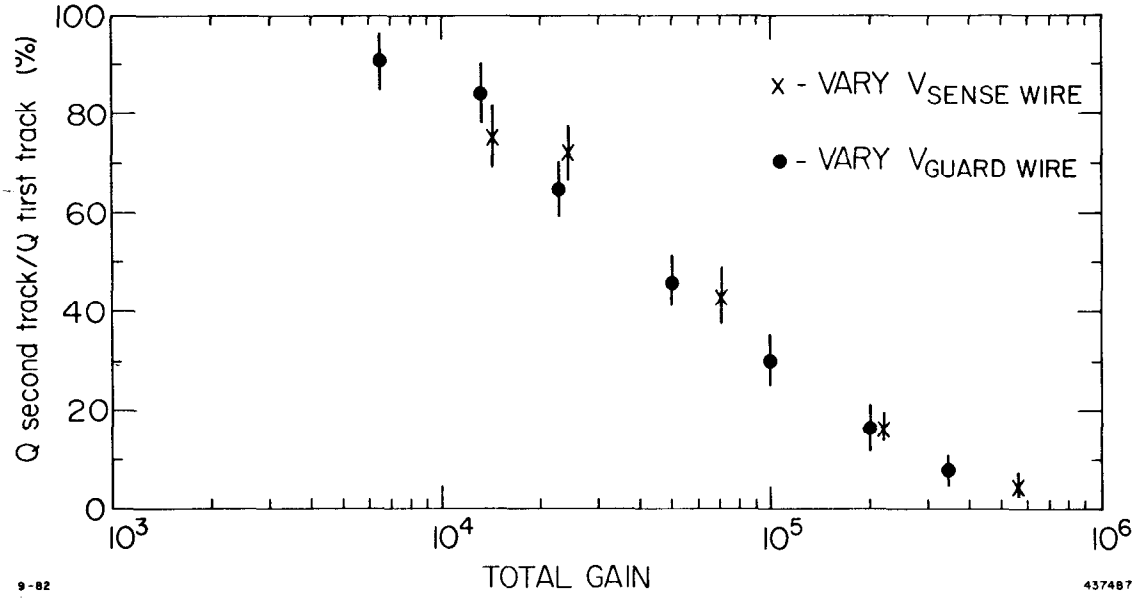
100
80
60
40
20
0
Q second track/Q first track (%)
x - VARY $V_{SENSE\ WIRE}$
● - VARY $V_{GUARD\ WIRE}$
10^3
10^4
10^5
10^6
TOTAL GAIN
9-82
437487

Fig. 14

MICRO-JET CHAMBER PROTOTYPE

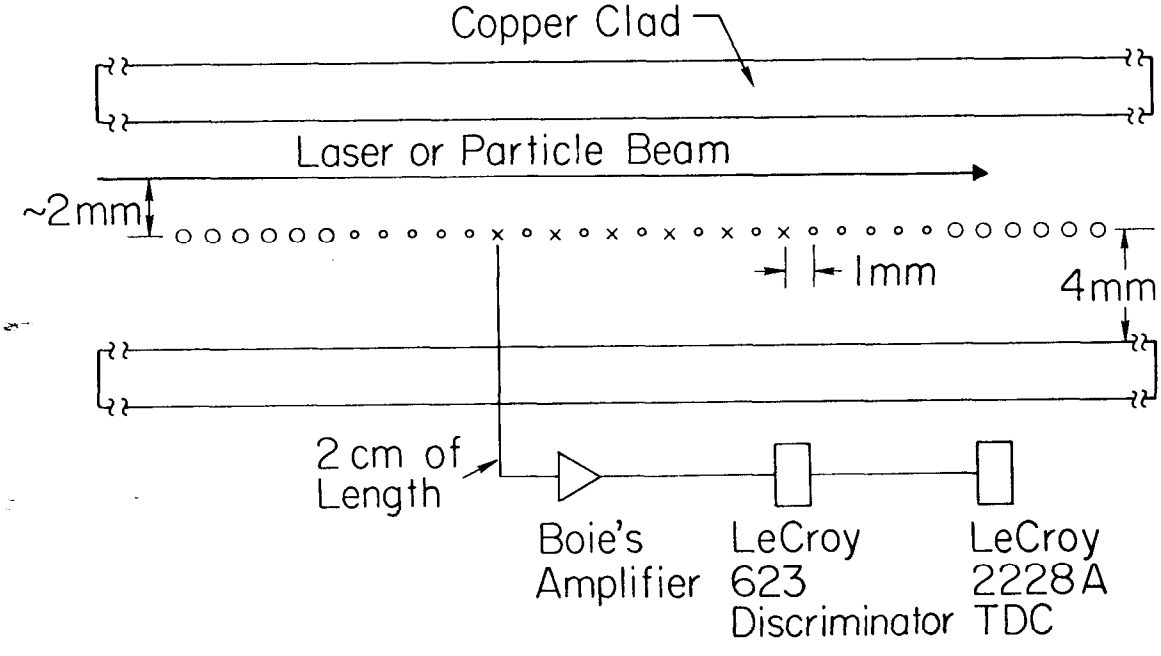

∘ ϕ 170 μm (Be-Cu) ∘ ϕ 100 μm (Be-Cu) × ϕ 7.8 μm (Au-W)

1-83 4367A16

Fig. 15

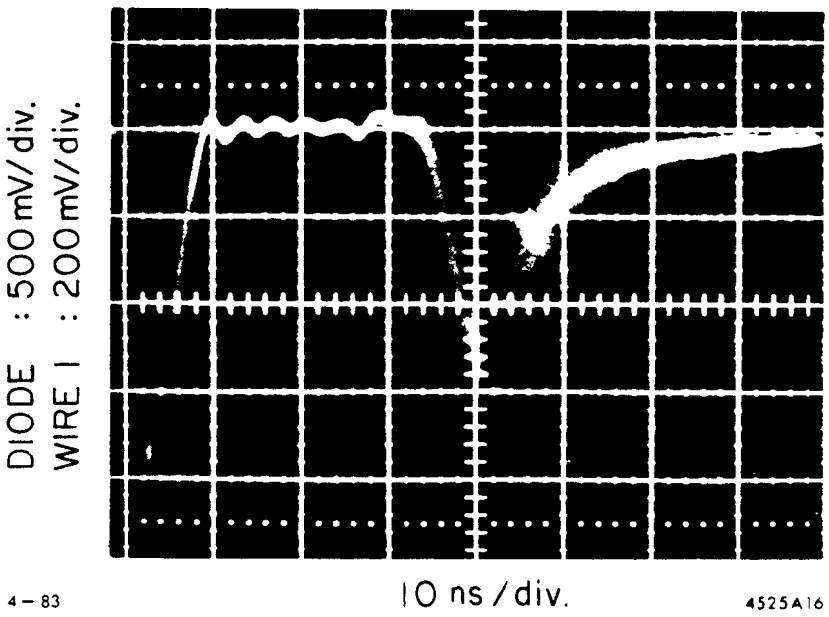

Fig. 16

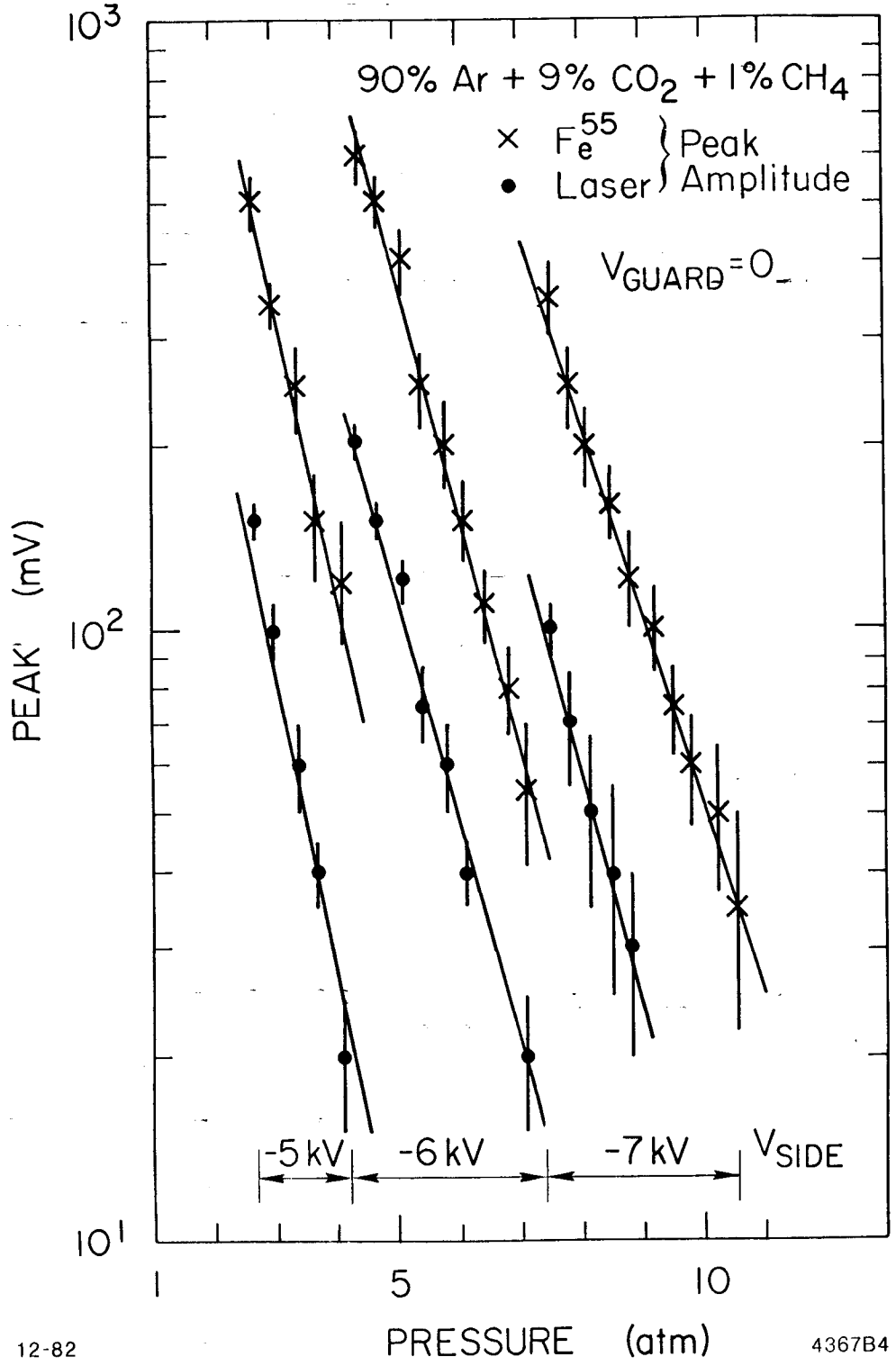
90% Ar + 9% CO_2 + 1% CH_4
× Fe^{55} } Peak
• Laser } Amplitude
V_{GUARD} = 0
-5 kV
-6 kV
-7 kV
V_{SIDE}
PEAK (mV)
10^3
10^2
10^1
1
5
10
PRESSURE (atm)
12-82
4367B4

Fig. 17

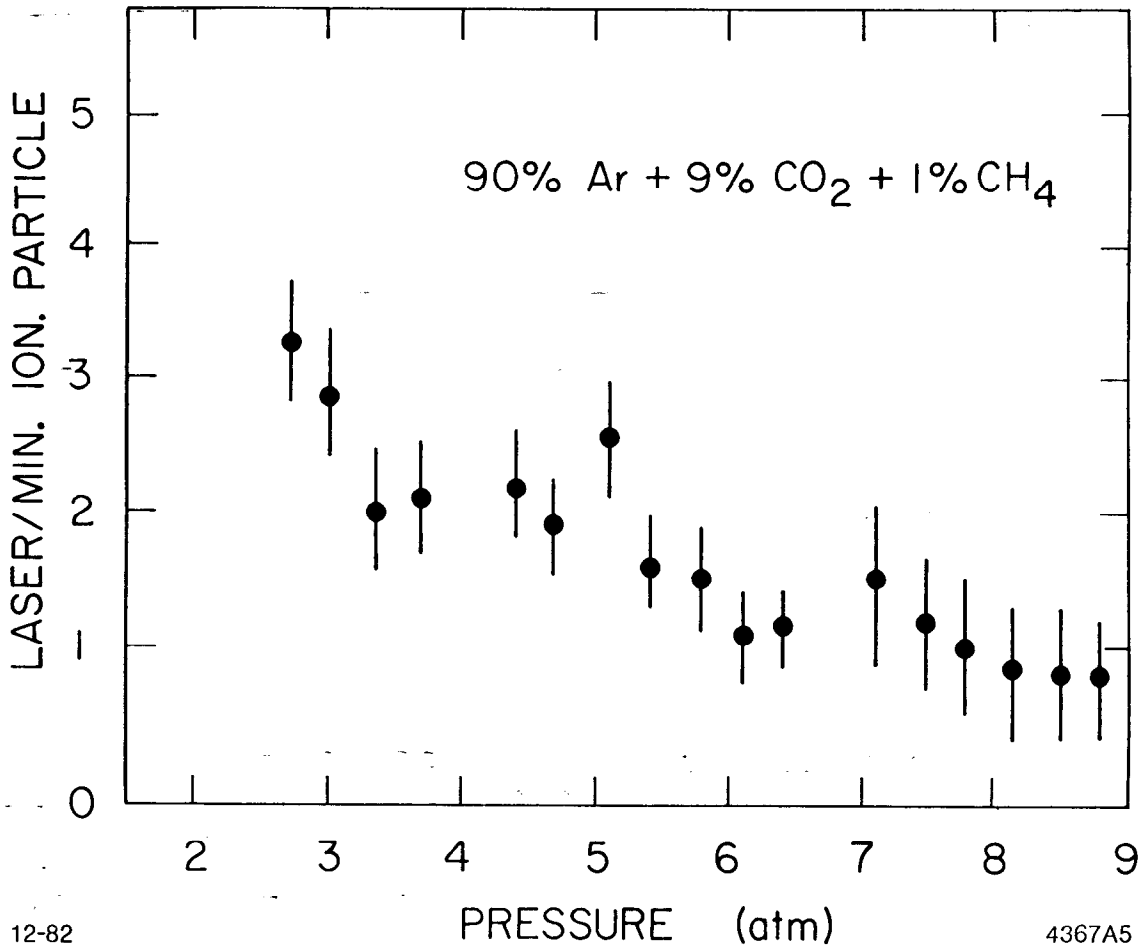
90% Ar + 9% CO_2 + 1% CH_4
LASER/MIN. ION. PARTICLE
0
1
2
3
4
5
2
3
4
5
6
7
8
9
PRESSURE (atm)
12-82
4367A5

Fig. 18

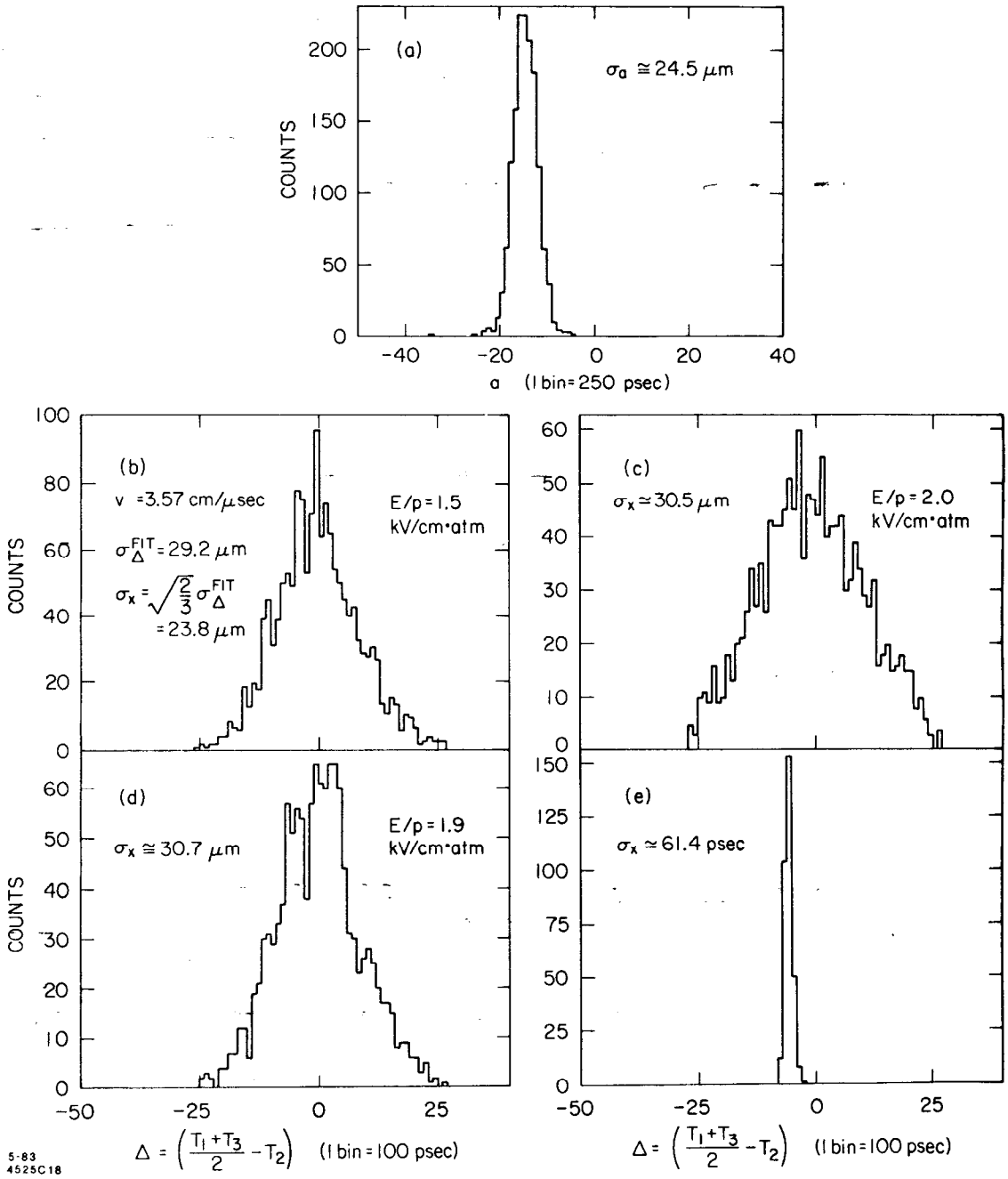
(a)
$\sigma_a \cong 24.5\ \mu m$
COUNTS
a (1 bin = 250 psec)
(b)
v = 3.57 cm/μsec
$\sigma_\Delta^{FIT} = 29.2\ \mu m$
$\sigma_x = \sqrt{\frac{2}{3}}\sigma_\Delta^{FIT} = 23.8\ \mu m$
E/p = 1.5 kV/cm·atm
(c)
$\sigma_x \simeq 30.5\ \mu m$
E/p = 2.0 kV/cm·atm
(d)
$\sigma_x \cong 30.7\ \mu m$
E/p = 1.9 kV/cm·atm
(e)
$\sigma_x \simeq 61.4$ psec
$\Delta = \left(\frac{T_1+T_3}{2} - T_2\right)$ (1 bin = 100 psec)
5-83
4525C18

Fig. 19